A combination dielectric and acoustic laboratory instrument for petrophysics

OPEN ACCESS
IOP Publishing
Measurement Science and Technology
Meas. Sci. Technol. **28** (2017) 125904 (19pp)
https://doi.org/10.1088/1361-6501/aa8cf3

A combination dielectric and acoustic laboratory instrument for petrophysics

Matthew Josh

CSIRO Energy, ARRC Laboratories Kensington, Perth 6151, Western Australia, Australia

E-mail: matthew.josh@csiro.au

Received 15 November 2016, revised 14 September 2017
Accepted for publication 15 September 2017
Published 22 November 2017

Abstract

Laboratory testing of rock samples is the primary method for establishing the physics models which relate the rock properties (i.e. porosity, fluid permeability, pore-fluid and saturation) essential to evaluating a hydrocarbon reservoir, to the physical properties (resistivity, nuclear magnetic resonance, dielectric permittivity and acoustic properties) which can be measured with borehole logging instrumentation. Rock samples usually require machining to produce a suitable geometry for each test as well as specific sample preparation, e.g. multiple levels of saturation and chemical treatments, and this leads to discrepancies in the condition of the sample between different tests. Ideally, multiphysics testing should occur on one sample simultaneously so that useful correlations between data sets can be more firmly established. The world's first dielectric and acoustic combination cell has been developed at CSIRO, so that a sample may be machined and prepared, then measured to determine the dielectric and acoustic properties simultaneously before atmospheric conditions in the laboratory affect the level of hydration in the sample. The dielectric measurement is performed using a conventional three-terminal parallel plate capacitor which can operate from 40 Hz up to 110 MHz, with modified electrodes incorporating a 4 MHz P-wave piezo crystal. Approximately 10 (acoustic P-) wavelengths interact with a typical (10 mm thick) sample so that the user may reliably 'pick' the P-wave arrival times with acceptable resolution. Experimental evidence indicates that the instrument is able to resolve 0.25 mm thickness in a Teflon sample test piece. For a number of engineering materials including Teflon and glass and also for a geological samples (Donnybrook sandstone from Western Australia) there is a perfectly linear relationship between both capacitance and P-wave arrival time with sample thickness. Donnybrook sandstone has a consistently linear increase in dielectric permittivity and P-wave velocity with saturation consistent with the Gassmann–Hill prediction. Both the dielectric permittivity and P-wave velocity are faster parallel to the bedding plane than orthogonal to the bedding plane in a shale from the Cooper Basin, Australia.

Keywords: dielectric permittivity, petrophysics, rock properties, acoustic properties, elastic properties

(Some figures may appear in colour only in the online journal)

Introduction

A variety of petrophysical and geophysical techniques are used in the petroleum industry for finding and evaluating strategic rock types that may play a role in hydrocarbon recovery. For example, remote sensing using seismic imaging to find and map potential targets in the subterranean topography is complemented by borehole logging techniques to determine more targeted physical information about the rock. Mineralogy, porosity, fluid permeability, pore-fluid type and saturation are all estimated from rock physical properties such as resistivity, seismic velocity, gamma radiation, neutron radiation and nuclear magnetic resonance (NMR).

Resistivity logging dates back to the very first borehole logs of the 1920s (Ellis and Singer 2007). Electrical conduction through a rock occurs partly through the rock matrix, but is dominated by the transport of charge carriers within the pore fluids leading to a contribution from both the porosity and pore connectivity as well as the type of pore fluid and the level of saturation. Low conductivity associated with a highly porous and permeable rock may be an indicator for the presence of hydrocarbons, but it may also be an indicator of low salinity. Dielectric logging was later introduced (Meador *et al* 1975a, 1975b) because water dipolar processes are less affected by an increase in salinity and water has a dielectric permittivity much higher than the dry rock matrix. Estimating the water-filled pore-space from a combination of dielectric permittivity and resistivity has been the subject of many rock models based on theory and experiment (Bruggeman 1935, Archie 1941, Hanai 1960, Sihvola 1999, Sen *et al* 1981, Asami 2002, Revil 2013). However, these models are somewhat complicated by a multitude of different electrical transport and polarisation processes (Guéguen and Palciaskas 1994). Archies equation relates the rock resistivity (R_t), to the porosity (ϕ), saturation (S_w), tortuosity factor (a) and brine resistivity (R_w) via a pair of simple exponents (Archie parameters, m, the cementation exponent and n, the saturation exponent), which need to be evaluated for the particular field or formation being investigated (Ellis and Singer 2007). The CRIM equation relates the effective dielectric permittivity of the formation (ε_{eff}) with ε_{ma} and ε_{rw} the rock matrix and pore fluid dielectric permittivities respectively and ε_h is the dielectric permittivity of gas.

$$R_t = a\varphi^{-m}S_w^{-n}R_w \quad \text{Archie's equation.} \tag{1a}$$

$$\sqrt{\varepsilon_{\text{eff}}} = \Phi S_w\sqrt{\varepsilon_{rw}} + \Phi\left(1 - S_w\right)\sqrt{\varepsilon_h} + \left(1 - \Phi\right)\sqrt{\varepsilon_{ma}} \quad \text{CRIM equation.} \tag{1b}$$

Simple mixing laws based on porosity and saturation (e.g. CRIM, Birchak *et al* (1974), are often used, but become complicated by long range dielectric processes in clay bearing rocks below 100 MHz (Fuller and Ward 1970, Revil 2013, Josh 2014, Josh and Clennell 2015, Josh *et al* 2016). Saturation also affects the acoustic properties, including the P-wave velocity, because water is less compressible and dense, than air or gas. Lebedev *et al* (2009) and Müller *et al* (2010) demonstrate that the relationship between saturation and P-wave velocity is not simple either and depending on pore connectivity and variable 'patchiness', different rocks may have completely different P-wave velocity to saturation profiles. Both compressional (primary or P-) wave and secondary (shear or S-) wave velocities are related to the mechanical rigidity of the rock and the density, but these are affected by the rock strength, confining pressure, mineralogy and pore-fluid. According to elastic theory (Gassmann 1951), P-wave velocity (V_{p}) is calculated from:

$$V_{\text{p}} = \sqrt{\frac{K + \frac{4}{3}\mu}{\rho}} \tag{2}$$

where K is the bulk modulus, μ is the shear modulus and ρ is the total rock density. The shear modulus is not affected as the saturation is increased, however the density does increase as the water fills the pore-space. The bulk modulus also increases with saturation because water is incompressible. The bulk modulus is complicated by the process of percolation and may rapidly increase as the percolation threshold is reached. As a result, the density and the bulk modulus may effect V_{p} differently in each rock sample, leading to a possible increase *or* decrease in V_{p} as the water content is increased and often not monotonically. For example, the Gassmann–Wood (GW) bound is valid when the characteristic patch size is small compared to the fluid diffusion length and the diffusion length is primarily controlled by rock permeability, fluid viscosity and acoustic wave frequency. Gassmann–Hill (GH) bound is valid when the patch size is much larger than the diffusion length and there is no pressure communication between the fluid pockets (Lebedev *et al* 2009). In the latter (GH) case, an increase in saturation leads to a monotonically, approximately linear increase in V_{p}. In the former (GW) case, V_{p} can decrease for the first half of the saturation profile (Müller *et al* 2010), then rapidly increases with additional saturation.

Technologies based on sensing rock physical properties in the petroleum industry are supported by laboratory analysis of rocks to establish the required models used to evaluate petrophysics log data using samples recovered by coring during drilling (Sen *et al* 1981, Mazzagatti *et al* 1983, Myers 1991, Seleznev *et al* 2011, Revil 2013). Achieving consistent models with laboratory experimentation is made difficult by the inhomogeneity of the rock and inconsistency with sample preparation (e.g. saturation). No two rock samples are exactly the same, even if the rock is perfectly isotropic and homogenous, two closely located samples may still be significantly different when comparing measurements such as dielectric permittivity and acoustic properties leading to scatter in the data. This is compounded by the requirement for different sample geometries in each of the testing methods. To address this challenge, a new combination dielectric and acoustic cell has been developed (Josh 2017) which allows both properties to be measured simultaneously from a relatively thin sample. Sample specific preparation routines such as hydration and chemical treatment are consistent at the time of measurement and are not altered by laboratory or storage conditions between dielectric and acoustic tests.

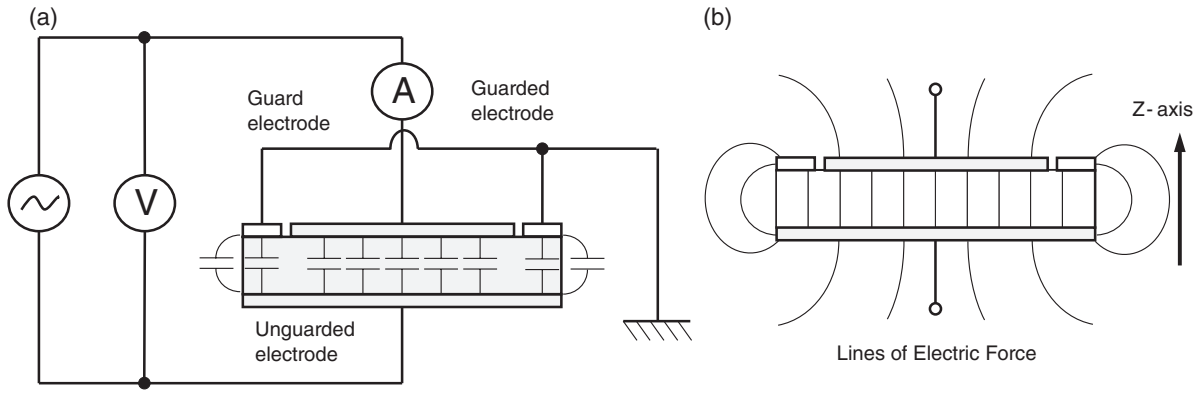

Figure 1. The conventional three-electrode (Von Hippel 1954) dielectric cell, redrawn from Keysight technologies 16451B dielectric test fixture manual (Keysight Technologies 2008). (a) The external circuit measures the impedance of the cell across the sample under test via the guarded electrode. (b) The guard electrode prevents stray (edge) current from being included in the sensitive region of the cell. The z-axis of the instrument is aligned with the sensing electric field vector.

Instrument design and theory

Dielectric measurement

The combination dielectric and acoustic cell is based on a 3-terminal dielectric cell (von Hippel 1954, Josh *et al* 2007, 2009, Keysight Technologies 2008), sometimes referred to as a guarded electrode arrangement figure 1, consisting of a simple parallel plate capacitor, modified to include an additional guard electrode surrounding one of the measuring (the guarded) electrodes. The stray edge capacitance is removed from the measurement of the sample under test using appropriate circuit connections to a four-terminal impedance analyser (Keysight Technologies 2017). The electric field in the guarded volume of the sample (figure 1(b)) is aligned with the z-axis (as marked) and is both uniform and parallel. Lumped element instruments of this style can achieve a significant increase in the upper frequency of operation by minimising the series inductance in the four-terminal electrode connections and this was achieved using small high frequency (mmcx) connectors which reduced the exposed length to approximately 1 mm. The instrument is attached to a 4-terminal impedance analyser (Agilent 4294A), and with suitable calibration the instrument can successfully produce reliable dielectric data up to the full 110 MHz limit of the impedance analyser.

The parallel capacitance and resistance of the guarded electrode to the unguarded electrode is measured and the dielectric permittivity and conductivity are calculated using:

$$\varepsilon^* = \varepsilon_0 \times \varepsilon_r^* = \varepsilon_0 \times (\varepsilon_r' - j\varepsilon_r'') \tag{3a}$$

$$\varepsilon_r' = \frac{C_p \times d}{\varepsilon_o \times A} \tag{3b}$$

$$\varepsilon_r'' = \frac{d}{2 \times \pi \times f \times \varepsilon_o \times R_p \times A} \tag{3c}$$

$$\sigma = \frac{d}{R_p \times A}. \tag{3d}$$

Where d is the thickness of the sample, A is the guarded plate area, f is the frequency, ε_r' and ε_r'' are the real and imaginary relative dielectric permittivities, ε_o is the permittivity of free space, σ is the conductivity, C_p and R_p are the measured parallel capacitance and resistance of the cell. Imaginary dielectric permittivity (ε_r'') and conductivity (σ) are physically different processes, the former relating to energy dissipation associated with driving dipolar processes and the latter associated with monopole translation and friction. Although they are *not* physically related, the two are mathematically interchangeable and often combined into a single parameter. In practice they are often distinguishable by their characteristic frequency response. The expressions (equations (3*a*)–(3*d*)) do not include the magnetic properties or imaginary conduction which *is* an explicit process in rock physics (Fuller and Ward 1970), but is sometimes lumped into the real permittivity.

Acoustic measurement

The unguarded and guarded electrode arrangements presented (figure 1) were each modified to incorporate a (PICeramics, 4 MHz) P-wave piezo transducer to form a dielectric-acoustic platen, with the ability to perform both the dielectric and acoustic measurements simultaneously (figure 2). The piezos were mounted within a screw tightening transducer housing (figure 3), assembled with coupling oil so that acoustic energy could be efficiently coupled through the platen into the sample. A high voltage is applied to one of the piezo crystals using an Olympus (5077PR) pulser-receiver (red, in figure 4) and the signal waveform received at the opposite piezo is amplified and captured by an oscilloscope.

Prior to the sample being inserted into the cell, the dielectric-acoustic platens are bare coupled together so that a zero-length P-wave arrival time, the so-called deadtime (blue in figure 4), can be recorded and subtracted from all subsequent measurements. The deadtime encapsulates all electronic signal propagation time through the cell and the connecting cables as well as any delays that occur within the pulser-receiver unit. The deadtime is captured by setting the first cursor (t_A) on the first wave arrival. After the sample is inserted, a new waveform is created (sample + deadtime, orange in figure 4) and a second cursor (t_B) is placed on the new first wave arrival. The direction of propagation of the P-wave is also aligned with the

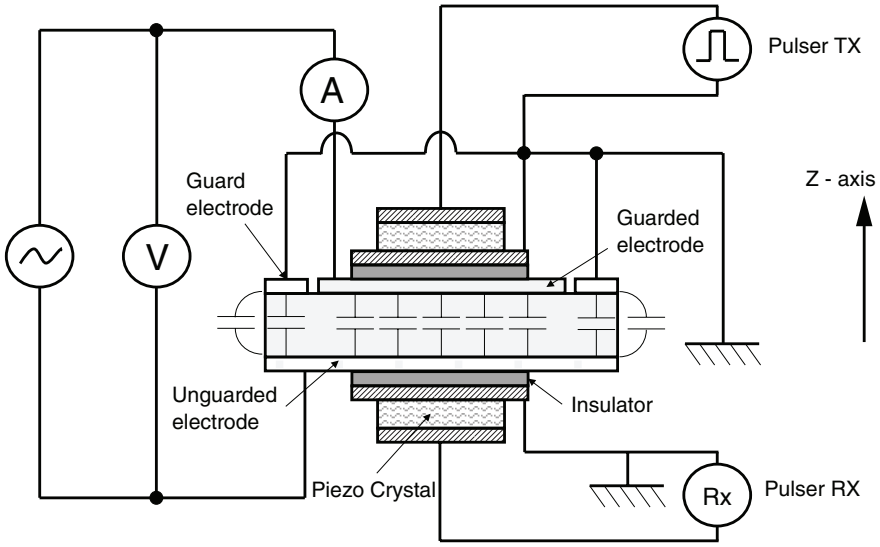

Figure 2. The circuit schematic of the combination dielectric and acoustic measurement cell. An impedance analyser is used for dielectric measurement and a pulser-receiver unit attached to an oscilloscope is used for the acoustic measurement. The z-axis is aligned with the sensing electric field vector as well as the wave vector of the P-wave, so that dielectric measurement is parallel to P-wave measurement.

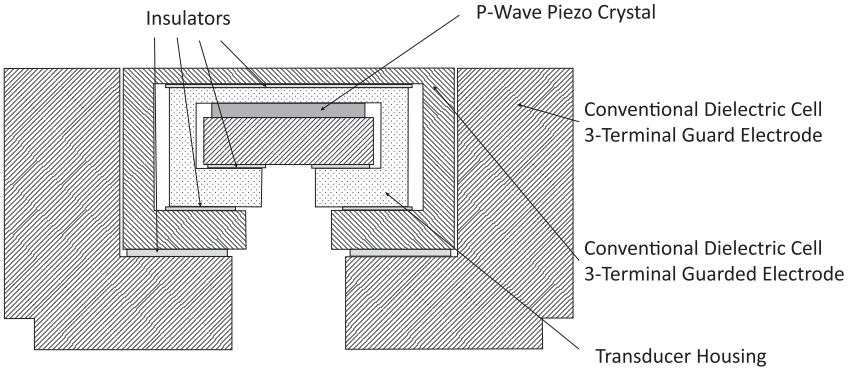

Figure 3. The sketches for the new combination dielectric-acoustic platens. The assembly consists of a transducer housing which contains the P-wave piezo placed inside the electrode assembly of a regular three-terminal capacitor.

z-axis of the cell. The transit time through the sample (Δt) can be calculated using:

$$\Delta t = t_B - t_A \tag{4a}$$

$$V_\mathrm{p} = \tilde{f}_\mathrm{c}\lambda = \frac{d}{\Delta t} \quad \therefore\ \lambda = \frac{d}{\tilde{f}_\mathrm{c} \times \Delta t} \tag{4b}$$

$$\text{Number of wavelengths} = \frac{d}{\lambda} = \Delta t \times \tilde{f}_\mathrm{c} \tag{4c}$$

where t_B is the sample captured wave arrival time, t_A is the deadtime wave arrival time, V_p is the P-wave velocity, $\bar{f}_\mathrm{c}$ is the piezo centre resonant frequency (different to f, the frequency of dielectric measurement equations (3a)–(3d)), d is the sample thickness and λ is the wavelength. Ideally at least 10 wavelengths should transit the sample (e.g. ASTM 2000) and this was achieved in most cases with the 4 MHz piezo, although a 10 MHz crystal was also tested, but it was more prone to cracking. Other piezo crystals were also considered, including an S-wave piezo, and this is a matter for future research.

Instrument housing and load cell

Other physical considerations included in the dielectric-acoustic instrument (figure 5) include: (1) the occasional necessity to apply significant stress to the sample. Sample loading *may* have an effect on the petrophysical behaviour of rock, particularly in cases where rocks are laminated and microfractured, this includes both uniaxial loading (in a simple case) or two- and three- axis confinement in more elaborate rock testing. Contact stress is also important in ultrasonics. Measurements presented in this investigation were made at 6.90 MPa uniaxial stress (or 1000 Psi); (2) It is often necessary to incorporate rock hydration, for example in the petroleum industry where dielectric permittivity is one of the accepted methods for distinguishing water filled pores from oil filled pores. The cell must therefore be enclosed so that water does not drain from the sample; (3) It may also be desirable to control the pore-pressure within the sample, but this was not attempted here.

The dielectric-acoustic platens are constrained within a pair of heavy stainless steel flange assemblies to achieve uniaxial

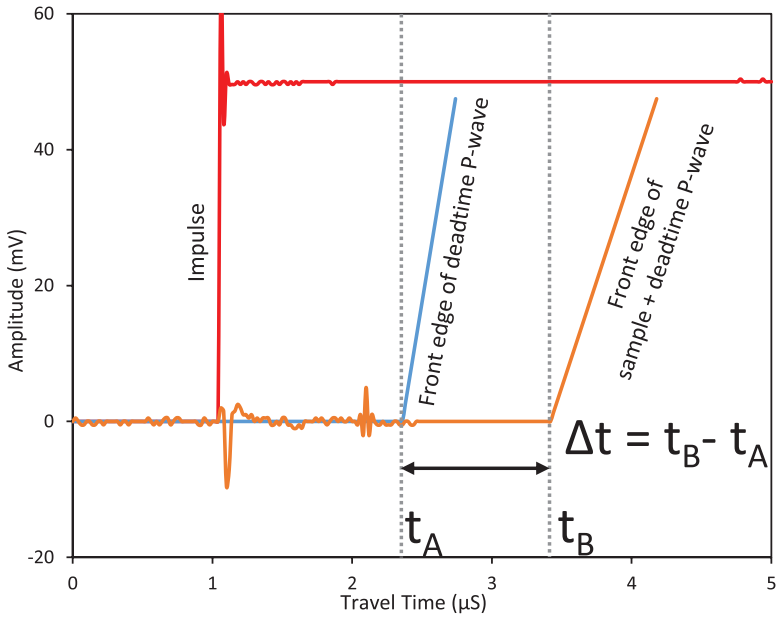

Figure 4. Cartoon of P-wave picking. The impulse signal (red) drives the piezo crystal transducers leading to a P-wave which propagates through the sample and is received via a piezo crystal in the opposite platen. The deadtime t_A is determined by coupling the bare platens together, and subsequent measurement of the rock is achieved by subtracting the deadtime from the arrival time t_B through the entire system and rock sample, to give the P-wave transit time through the sample only Δt.

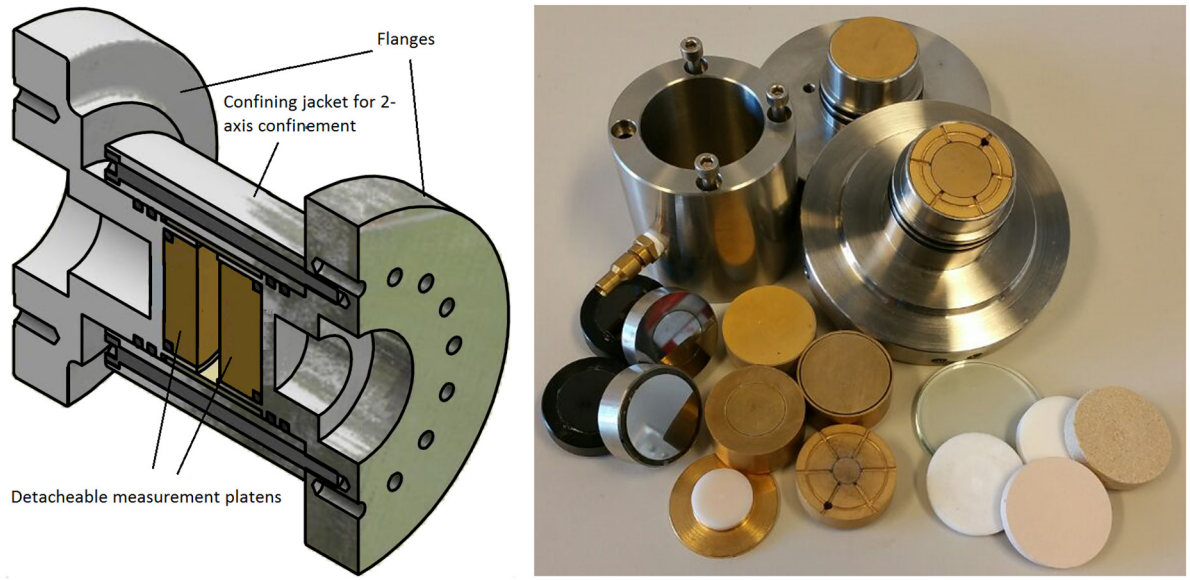

Figure 5. (a) Sketch and (b) photo of the dielectric and acoustic measurement cell. Consisting of a pair of flanges with the detachable measurement platens (orange in the sketch and gold plated brass in photo), which can be re-configured and interchanged for different sample sizes and measurement purposes. Glassy carbon, pyrol and platinum black platens can also be used to overcome electrode polarisation (Ishai *et al* 2013). The platens may consist of simple dielectric cell modules or combination dielectric-acoustic platens as presented here. The example test samples in the bottom right of the photo include a glass, an alumina and two Teflon standard reference pieces as well as one geological example (Donnybrook sandstone).

confinement and a nitrile sleeve inside a pressure housing was used to achieve confining pressure. The instrument was adapted to fit into a pre-existing custom built load cell (Siggins *et al* 2011), The port on the side of the pressure sleeve (visible in the photo figure 5 can have air, water or oil attached, to increase the pressure between the pressure housing and the flexible nitrile sleeve to confine the rock sample.

Platen physics

Inside the cell assembly, the dielectric-acoustic platens can be quickly removed or swapped if irregular samples are being analysed. A variety of interchangeable platens have been manufactured. For example, if only small fragments of rock are available then it is still possible to achieve dielectric-acoustic analysis of the intact rock, if parallel faces can be prepared

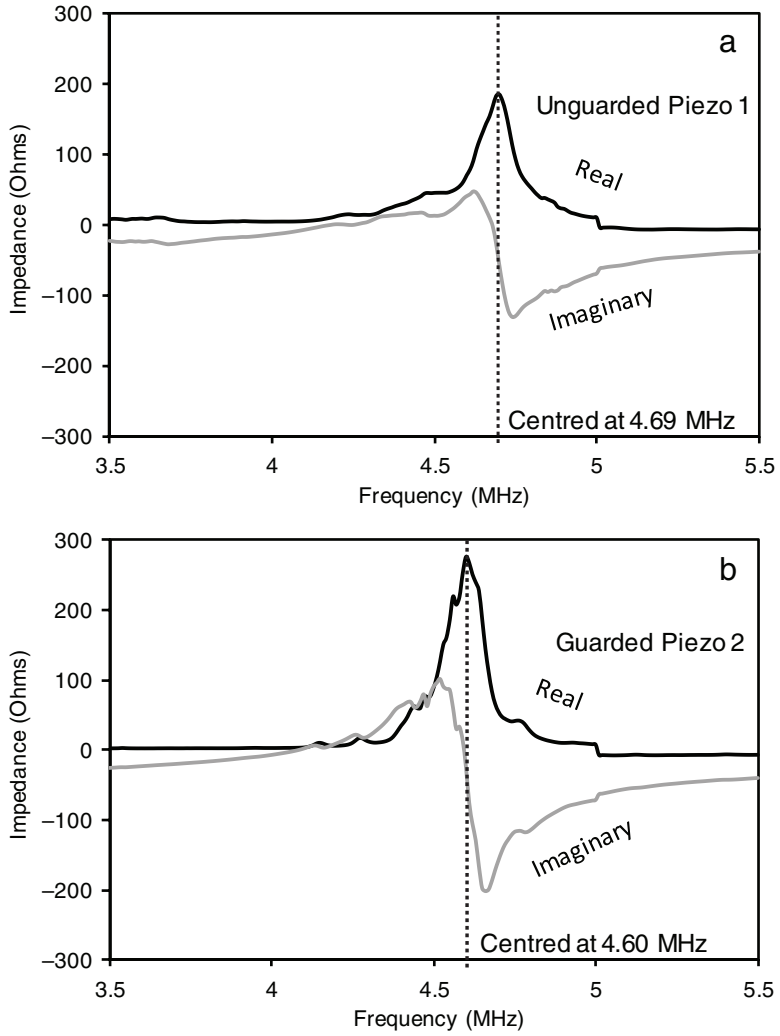

Figure 6. The real and imaginary impedance of the (a) unguarded and (b) guarded, acoustic transducer assemblies. The unguarded transducer characteristic resonant frequency peak occurs at $\tilde{f}_c = 4.69$ MHz. The guarded transducer characteristic resonant frequency peak occurs at $\tilde{f}_c = 4.60$ MHz.

and a small diameter platen is used. Likewise physical limitation in the measurement of the sample may lead to alternative electrode materials. For example, electrode polarisation, which occurs during the testing of lossy geological samples such as clay bearing rocks and shales (Malleo *et al* 2010, Ishai *et al* 2013), may be significantly improved through the use of glassy carbon, pyrol, platinum black and other electrode types. Electrode polarisation is slightly improved through electrode surface roughening using a lapping process and in the present configuration, gold plated lapped brass was the material chosen.

Sample preparation

A combination of engineering standard reference materials and petroleum reservoir rock types including shale and sandstone were tested in the dielectric-acoustic cell. Engineering reference materials included soda-lime glass and Teflon, because they have consistent and well characterised acoustic and dielectric properties. Multiple thicknesses were prepared to confirm the relationship between plate separation and capacitance and conductance predicted by equations (3*a*)–(3*d*). Additional engineering reference materials with published dielectric and acoustic properties were also tested to compare measurements with other commercially available systems. Typical petroleum industry geological samples included a shale from the Cooper Basin, Australia and Donnybrook sandstone from a quarry approximately 200 km south of Perth, Australia. Donnybrook sandstone is well cemented, stable and easily machined, but also quite homogenous and isotropic, so it was also used to perform a multi-thickness experiment alongside the engineering materials.

The samples were prepared as thin slices with precision ground faces having a tolerance of 30 μm variation in thickness achieved using a diamond surface grinder and large enough to cover the unguarded electrode diameter of 37 mm. In the case of the geological samples, additional processes were used in each case to achieve varying levels of hydration. Anisotropy of the dielectric permittivity and acoustic properties was measured for the shale samples by producing two samples of each shale, one cut with the bedding oriented parallel to the z-axis of the dielectric-acoustic cell (figures 1 and 2) and the other cut with the bedding oriented perpendicular to

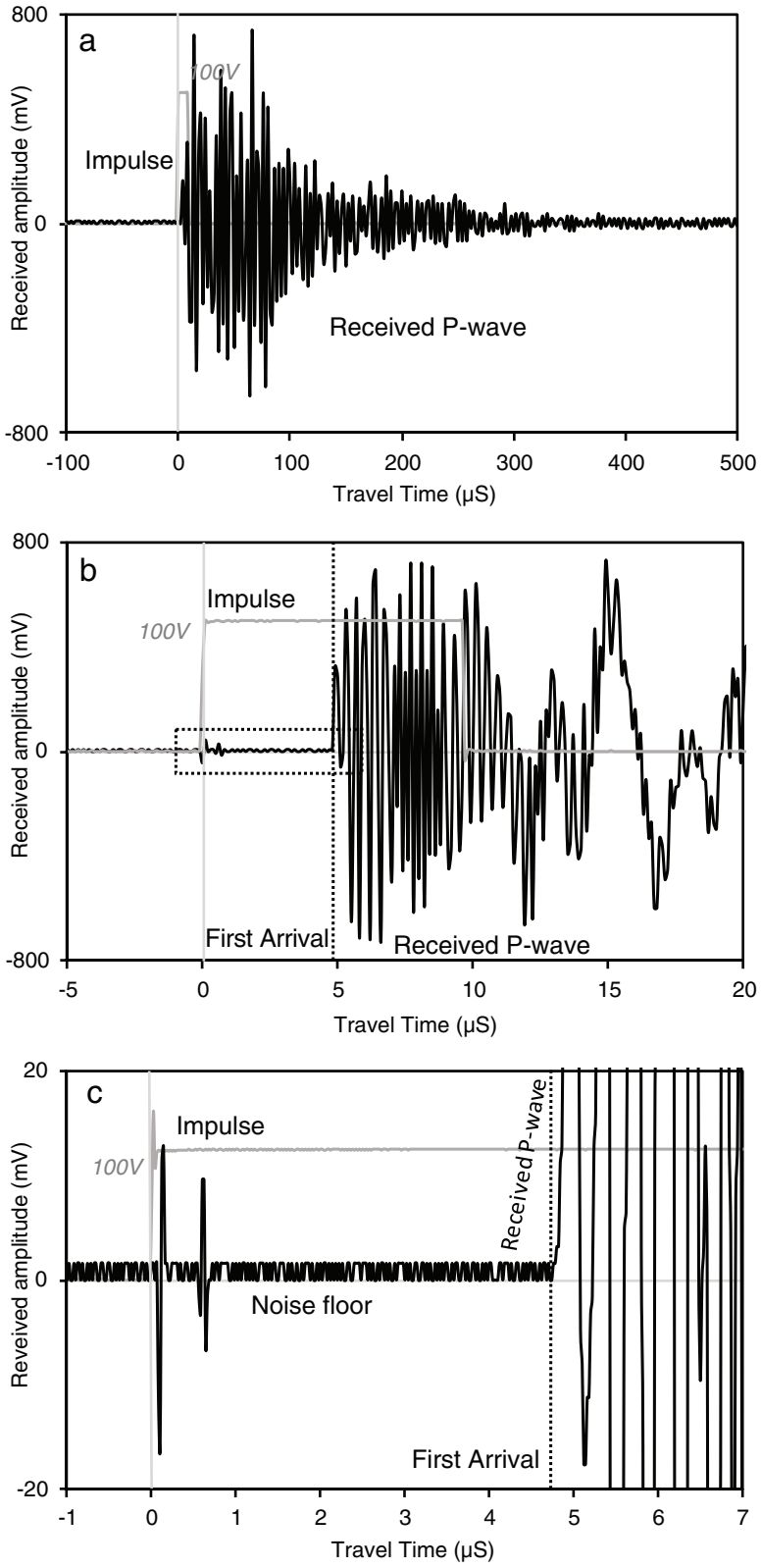

Figure 7. Captured P-wave arrival through a sample (a) at full scale (b) partially zoomed in and (c) zoomed in to show P-wave arrival pick. In each trace the grey curve is the impulse signal driving the piezo crystals, the black curve is the P-wave as received. The full P-wave capture (a) occurs as a sharp ringing oscillation which decays over approximately 300 μs. The front edge (c) is where a rapid departure from the approximately flat (although a little noisy) trace, at approximately 4.8 μs, and is recorded as the P-wave first arrival. The rapid spikes occurring at approximately 0.1 and 0.6 μs are cross talk occurring in the high voltage circuits, however it occurs before the P-wave arrival and does not interfere with the P-wave pick.

Table 1. Three sample materials, Teflon, soda-lime glass and Donnybrook sandstone (a natural geological material) were prepared in multiple thicknesses. Capacitance and resistance at 10 MHz have been tabulated and these scale proportionally to the sample thickness (capacitance inversely). Likewise the P-wave travel time increases with sample thickness for each sample type.

Sample	Sample thickness (mm)	P-wave travel time (nS)	P-wave velocity, V_p (m s^{-1})	Number of wavelengths	Capacitance at 10 MHz (pF)	Resistance at 10 MHz (Ω)	Real relative dielectric permittivity, ε_r at 10 MHz	Conductivity (S m^{-1})
TeflonA_1	0.25	160.00	1562.50	0.74	26.03	4.528	2.03	1.521×10^{-13}
TeflonB_1	0.50	360.00	1388.89	1.66	12.90	5.041	2.01	2.732×10^{-13}
TeflonC_1	1.99	1400.00	1421.43	6.44	3.43	2.129×10^{1}	2.12	2.575×10^{-13}
TeflonD_1	4.99	3560.00	1401.69	16.38	1.35	1.808×10^{2}	2.10	7.602×10^{-14}
Soda-limeA_1	2.10	360.00	5833.33	1.66	11.04	1.915×10^{-1}	7.22	3.021×10^{-11}
Soda-limeB_1	2.86	520.00	5500.00	2.39	8.17	2.614×10^{-1}	7.28	3.013×10^{-11}
Soda-limeC_1	5.14	900.00	5711.11	4.14	4.47	4.703×10^{-1}	7.15	3.011×10^{-11}
Soda-limeD_1	9.83	1720.00	5715.12	7.91	2.26	8.782×10^{-1}	6.92	3.083×10^{-11}
DonnybrookA_1	3.18	1000.00	3180.00	4.60	6.70	5.728×10^{-3}	6.63	1.529×10^{-9}
DonnybrookB_1	4.74	1400.00	3385.71	6.44	4.41	1.004×10^{-2}	6.50	1.301×10^{-9}
DonnybrookC_1	5.08	1400.00	3628.57	6.44	4.24	8.436×10^{-3}	6.71	1.659×10^{-9}
DonnybrookD_1	6.08	1760.00	3454.55	8.10	3.76	8.883×10^{-3}	7.12	1.885×10^{-9}
DonnybrookE_1	8.91	2480.00	3592.74	11.41	2.49	1.266×10^{-2}	6.90	1.938×10^{-9}
DonnybrookF_1	9.68	2560.00	3781.25	11.78	2.18	1.716×10^{-2}	6.56	1.554×10^{-9}

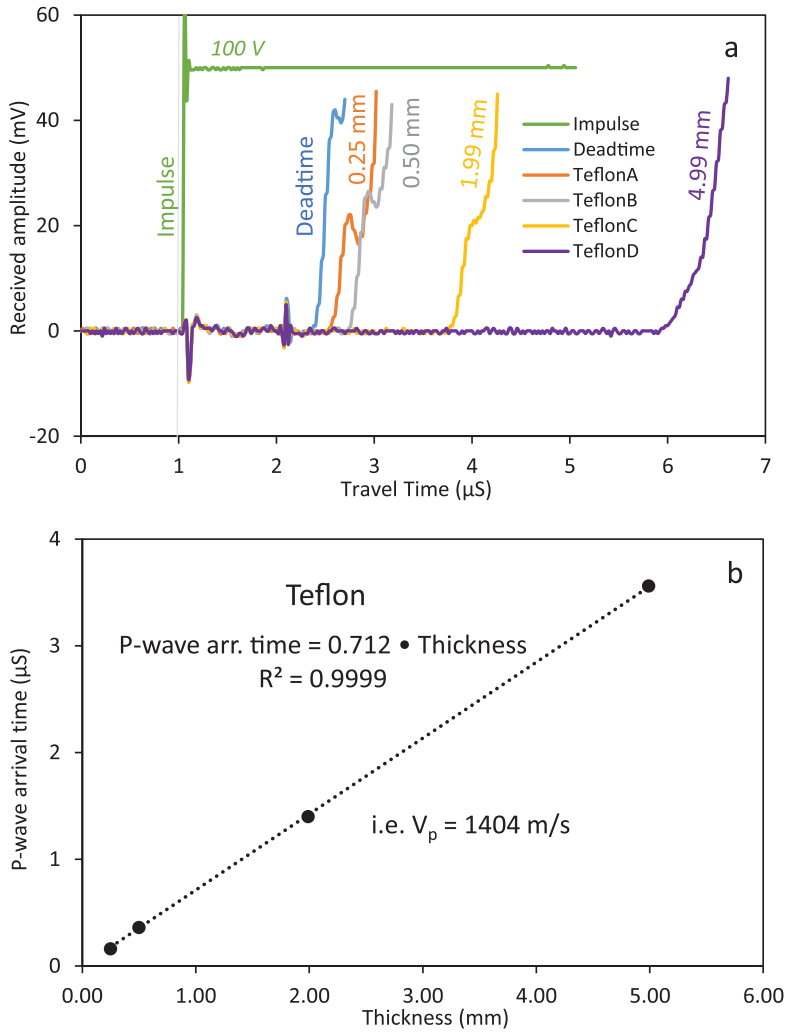

Figure 8. (a) P-wave arrivals through four different thicknesses of Teflon along with the zero-length deadtime arrival (blue). Thicker samples consistently lead to a longer arrival time. (b) The sample P-wave transit time is nearly perfectly correlated ($R^2 = 0.9999$) with the thickness of the sample.

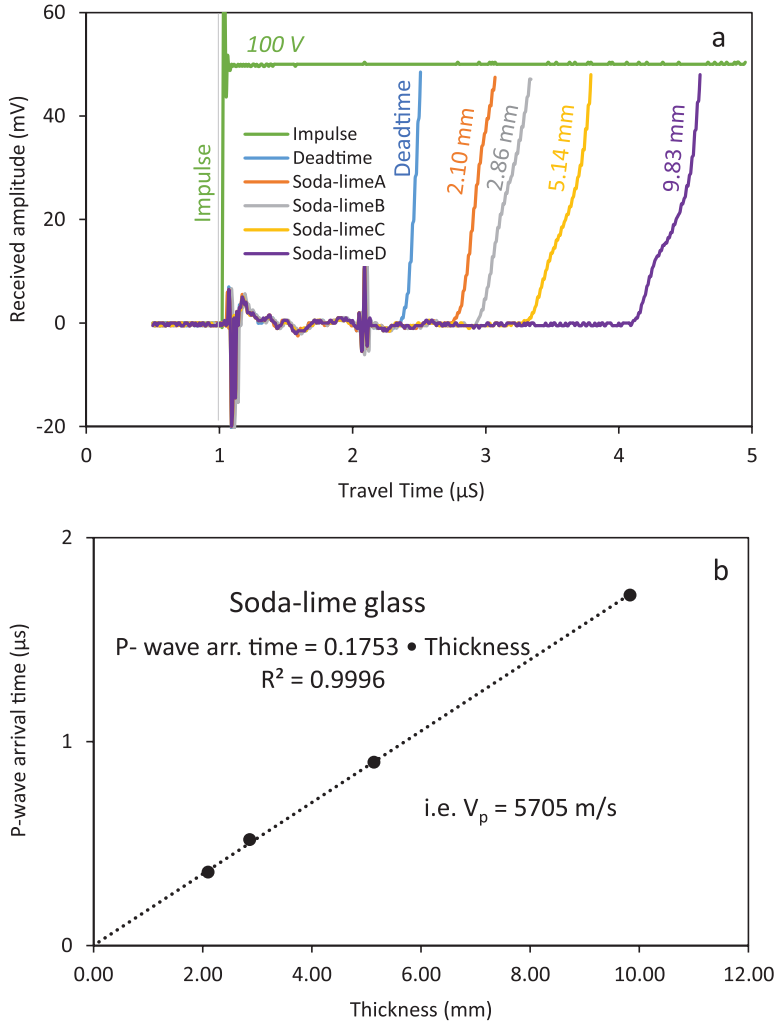

Figure 9. (a) P-wave arrivals through four different thicknesses of soda-lime glass along with the zero-length deadtime arrival (blue). Thicker samples consistently lead to a longer arrival time. (b) The sample P-wave transit time is nearly perfectly correlated ($R^2 = 0.9996$) with the thickness of the samples.

the z-axis of the dielectric-acoustic cell. The sandstone had a coarser grain size and larger pores, so moisture was easily added to the sample by evacuation followed by immersion, then removed from the sample by placing the saturated sample on a vacuum Buchner funnel and drawing a vacuum through the sample. Shale samples are more problematic because they have very small pores, but stabilising the shales in desiccator with a constant humidity (Josh *et al* 2016) for 3 weeks prior to the dielectric-acoustic measurement, proved successful. The baked dry mass of the sample ($\text{mass}_{\text{baked}}$) was recorded along with the saturated mass ($\text{mass}_{\text{saturated}}$) and the mass occurring during analysis (mass), and these were used to calculate the saturation (S_w), using:

$$\text{mass}_{\text{water}} = \text{mass} - \text{mass}_{\text{baked}} \tag{5a}$$

$$\text{Water content}_{\text{by mass}} = 100 \times \frac{\text{mass}_{\text{water}}}{\text{mass}} \tag{5b}$$

$$\text{Saturation}, S_w = 100 \times \frac{\text{mass}_{\text{water}}}{\text{mass}_{\text{saturated}} - \text{mass}_{\text{baked}}} = 100 \times \frac{\text{mass} - \text{mass}_{\text{baked}}}{\text{mass}_{\text{saturated}} - \text{mass}_{\text{baked}}}. \tag{5c}$$

Given that the porosity of the rock (ϕ) and the density of the rock matrix and water do not change for a given sample, m_{water}, could be used to calculate the porosity and the water content by volume. It must also be noted that a water-mass based method works acceptably for sandstones because they have large well connected pores. Other rock types (e.g. shales) require more dedicated methods such as helium porosimetry and pycnometry which use a more penetrating fluid to interrogate the tight pore-space.

Results and discussion

Acoustic transducer frequency response

The centre resonant frequency of the (arbitrarily 4 MHz) piezo crystals was determined precisely using an impedance analyser to capture the air coupled frequency response. The individual unguarded and guarded dielectric-acoustic platens were both tested (figure 6) and found to have centre resonant frequencies of $\tilde{f}_c = 4.69$ MHz (unguarded) and $\tilde{f}_c = 4.60$ MHz (guarded). The lower of the two i.e. 4.60 MHz was used

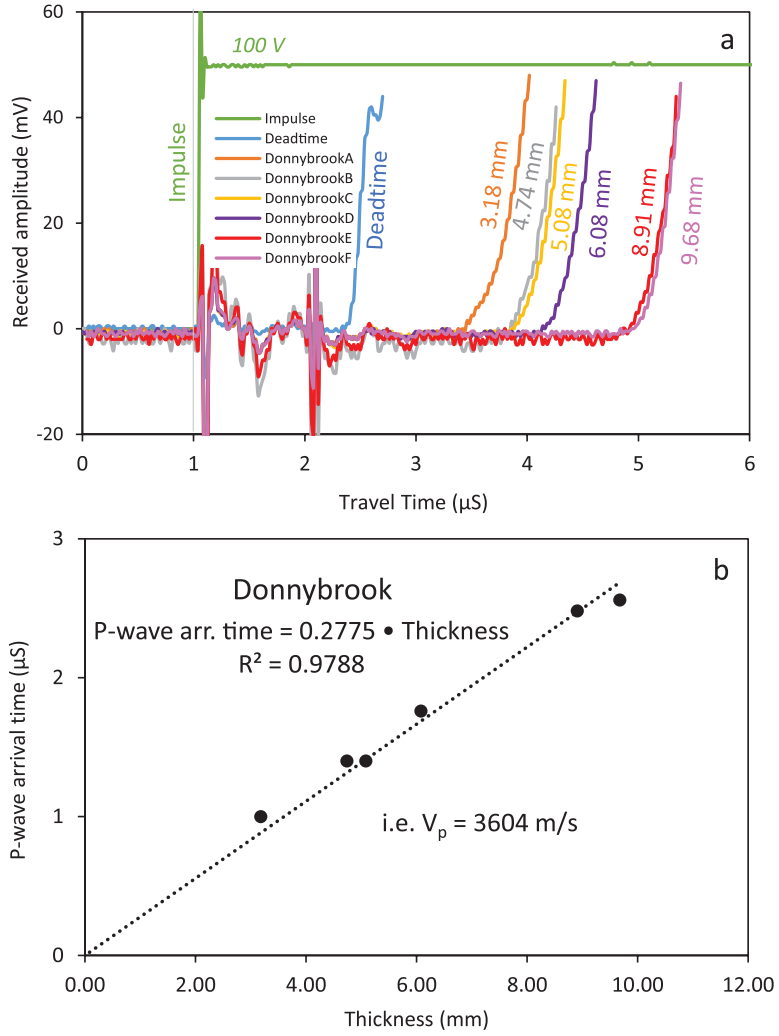

Figure 10. (a) P-wave arrivals through six different thicknesses of Donnybrook sandstone along with the zero-length deadtime arrival (blue). Thicker samples consistently lead to a longer arrival time. (b) The sample P-wave transit time is nearly perfectly correlated ($R^2 = 0.9788$) with the thickness of the samples but very slightly weaker than the engineering materials.

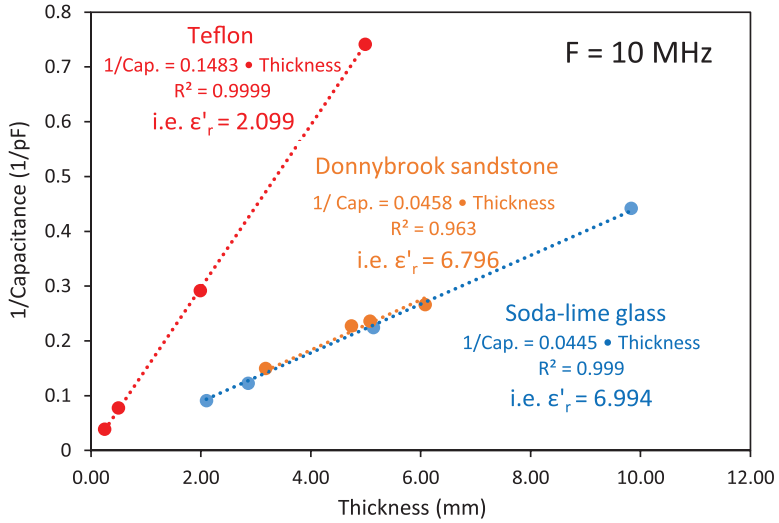

Figure 11. The inverse of the capacitance increases linearly ($R^2 > 0.99$) with an increase in sample thickness for all sample materials.

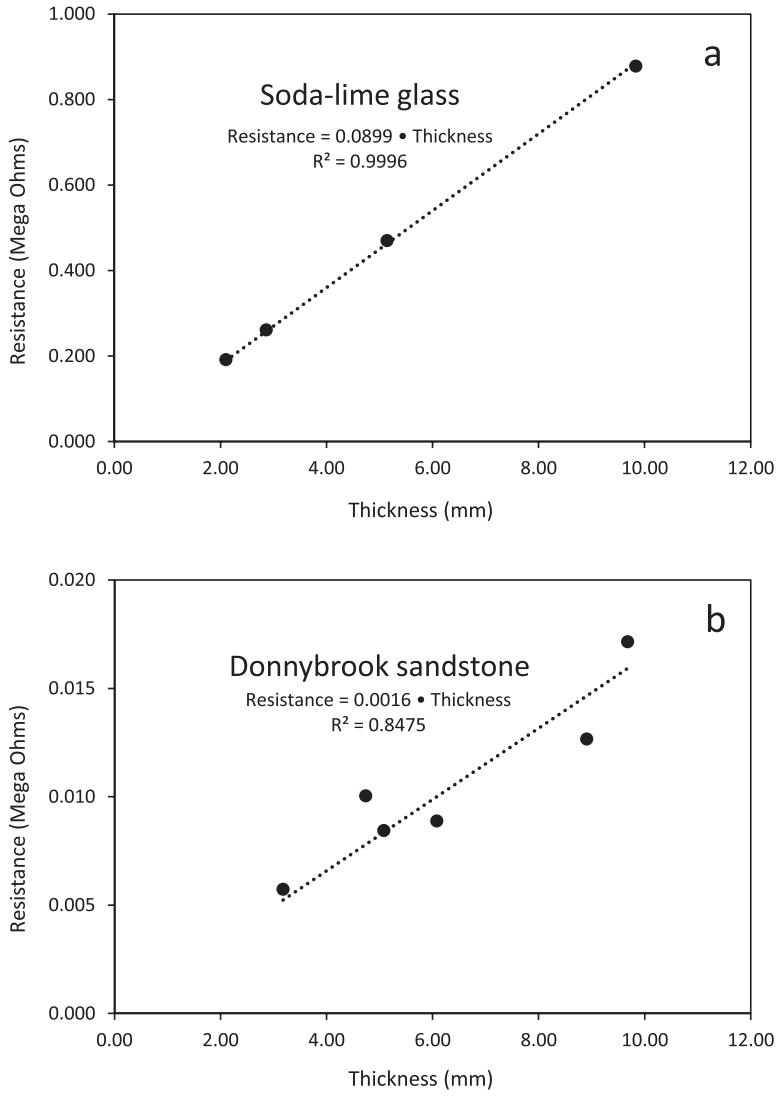

Figure 12. The resistance of the soda-lime glass (a) correlates very consistently with the sample thickness ($R^2 > 0.999$) typically in the range of 200 KΩ up to 1 MΩ, which is well suited for the impedance analyser used. Donnybrook sandstone however (b) exhibited a lower resistance of 5–20 KΩ, but variations within the geological sample have led to a weakening of the correlation of ($R^2 = 0.8475$). The Teflon sample had an ultra-high resistance which was outside the measurable range of the impedance analyser.

with equation (4*c*) to determine the number of wavelengths occurring in a given sample.

Multi-thickness experiments

During the experiment, the acoustic arrival signals were automatically captured (figure 7); however, the acoustic P-wave arrival was more easily picked directly off the oscilloscope during the measurement process (recorded in table 1) and used with the sample thickness to determine the P-wave velocity (V_p). In the example presented in figure 7). The complete P-wave is provided for a Donnybrook sandstone sample demonstrating that the P-wave received after the impulse contains a long period of oscillation which decays after approximately 300 μs. By zooming in on the front edge of the P-wave arrival it is possible to 'pick' the front edge, by subjectively choosing when the received signal departs significantly from the noise floor.

In the examples shown here (table 1), the number of wavelengths interacting with the sample is lower than 10, but this is mainly occurring for samples less than 8 mm thick and for soda-lime glass with a V_p of 5700 m s^{-1} which is much higher than the geological examples. For the geological samples (for which the instrument has been designed) greater than 8 mm thick, the problem is significantly reduced and the number of wavelength within the sample exceeds 10.

The individual measurements of P-wave velocity at 4.6 MHz, tabulated in table 1 are consistent with values published in the ultrasonic velocity table (Advanced NDT Ltd), which include 5766 m s^{-1} for soda-lime glass and 1372 m s^{-1} for Teflon. However, the P-wave velocity determined from the global dataset for each sample type (figures 8–10), has been determined from the gradient of the P-wave arrival time versus the sample thickness. Teflon was experimentally determined to have a P-wave velocity of 1404 m s^{-1}, the soda-lime

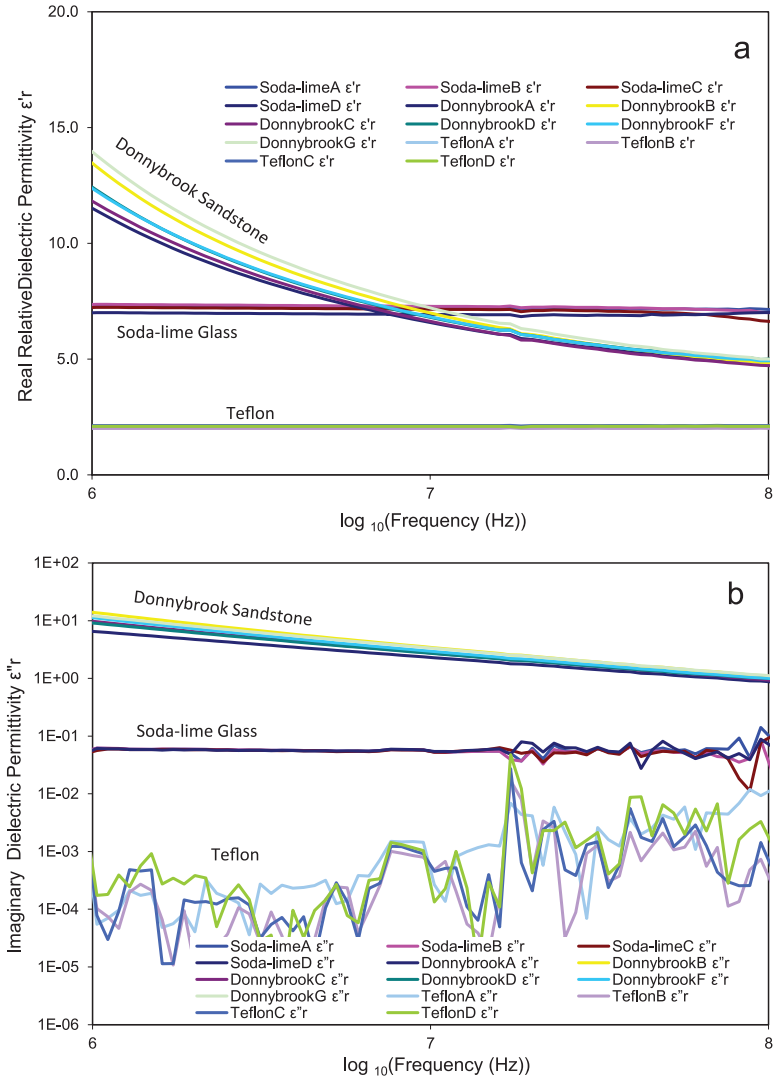

Figure 13. The complete electrical transport properties spectra from 1 MHz up to 100 MHz for the Teflon, soda-lime glass and Donnybrook sandstone samples. (a) The real and (b) imaginary relative dielectric permittivity of the samples. Teflon has a very low real relative dielectric permittivity of 2.1 (see 2.1 in the literature also) and a conductivity below the range of sensitivity of the impedance analyser. Soda-lime glass has a very high dielectric permittivity of approximately 7, which decreases slightly with frequency (i.e. it is dispersive). But by far the most conductive and highly dispersive is the Donnybrook sandstone, which has a real relative dielectric permittivity at 1 MHz between 11.5 and 13 reducing to approximately 5 at 100 MHz.

glass was 5705 m s^{-1} and the Donnybrook sandstone was 3603 m s^{-1}. The variation in the P-wave velocity of the Donnybrook sandstone samples (A; 3180 m s^{-1} compared to F; 3781 m s^{-1}) is likely to be caused by small geological variations in the samples and possibly the porosity and hydration of the samples, but these variations are smaller in the engineering materials because they are more homogenous, less porous and less prone to atmospheric variations in humidity. It is most remarkable that this instrument is able to resolve P-wave transit time through samples as thin as 0.25 mm.

The dielectric permittivity measured for the different Teflon test pieces at 10 MHz (table 1), is generally between 2.00 and 2.23 which matches the accepted published values (von Hippel 1954). The soda-lime glass test pieces exhibit dielectric permittivities between 6.9 and 7.3 and Donnybrook sandstone samples are between 6.5 and 7.11 at the same frequency. The inverse capacitances for the dielectric-acoustic cell for each of the sample types, varies perfectly linearly with the thickness of the sample (figure 11) and consistently with equations (3*a*)–(3*d*), the gradient of which is used to calculate global dielectric permittivities of 2.099 for Teflon, 6.796 for Donnybrook sandstone and 6.994 for soda-lime glass, at the measurement frequency of 10 MHz tabulated in table 1.

Similarly the correlation between the resistance and the sample thickness (figure 12) is also generally strong if the sample falls within the operating limits of the impedance analyser (refer to Keysight Technologies 2017) and where a guaranteed homogenous and isotropic engineering material such as polymer or glass is tested. In the case of geological materials, the correlation appears to exhibit some weakening due to less certainty about the exact state of the sample during the test and whether they are homogenous, but the correlation is still $R^2 = 0.85$, and this would be considered to be quite strong in petrophysics.

Table 2. P-wave velocity and dielectric permittivity for a number of engineering materials. Samples were measured using the present instrument (Measured) and compared with measured data from a commercial comparison instrument (Comparison). Where available, published values are also provided with any available information on sample variation[2].

	P-wave velocity, V_p (m s^{-1})			Real relative dielectric permittivity at 10 MHz		
	Measured	Comparison	Published	Measured	Comparison	Published
Metal						
Aluminium (7075-T6)			6350 (R), 6320 (Olymp.), 6300			
Titanium	6053	5734	6100 (R), 6172 (Adv. NDT, 6Al–4V), 6100 (Olymp.), 6100 (A), 6100(Q)			
Inconel625	5859	5565	5820 (R), 7823 (Adv. NDT, Wrought), 5820 (Olymp.)			
Stainless Steel (304)	5780	5444	5660 (R), 5613–5740 (Adv. NDT), 5740 (Olymp., SS 302), 5900 (A, type unknown)			
Brass (Navel)	4583	4476	4430 (R), 4369 (Adv. NDT, 70%–30%), 4430 (Olymp.), 4700 (70–30 A), 4300 (Q)			
Copper	4670	4558	4660 (R), 4750 (Adv. NDT), 4660 (Olymp.), 4701 (Rae and Brown2016), 4700 (Q)			
Aluminium (6061-T6)	6360	6079	6299 (Adv. NDT, 6061-T6), 6442 (Rae and Brown 2016)			
Aluminium (5000 series)	6442	5997				
Mild Steel	5767	5571	5900 (Q)			
Polymers						
PVC (grey)	2462	2354	2330 (R), 2395 (Olymp.), 2380 (A), 2380 (Grey, B)	3.12	3.16	3.4 (D), 3.2–3.5 (1Mhz F),
Polycarbonate	2271	2222	2286 (Adv. NDT), 2213 (Rae and Brown 2016), 2270 (A), 2270 (B)	2.92	2.96	3.0 (D), 3.17 (1 MHz, G), 2.96 (Lexan, H)
Nylon 6/6	2801	2697	2692 (Adv. NDT), 2600 (Olymp.), 2600, (6/6, A), 2600 (6/6 B)	3.28	3.33	4–5 (D), 3.3 (1 MH 6/6 F)
PTFE (Teflon)	1398	1336	1400 (R), 1372 (Adv. NDT),1312 (Rae and Brown 2016),	2.08	2.12	2.0–2.1 (D)
HDPE (Polyethelene)	2508	2445	2667 (Adv. NDT), 2460 (Olymp.), 2628 (Rae and Brown 2016), 2430 (A), 2430 (B)	2.41	2.43	2.2–2.4 (D),
Polypropylene	2707	2640	2470 (A), 2660 (B)	2.31	2.35	1.5 (D), 2.2 (H)
Plexglass (Acrylic Perspex)	2757	2719	2760 (R), 2730 (Olymp.), 2750 (A)	2.76	2.81	2.76 (1 Mhz F)
PEEK	2610	2548	2581 (Rae and Brown 2016)	3.24	3.29	3.3 (1 MHz, S)
Acetal (Delrin)	2340	2364	2430 (A), 2430 (B)	3.62	3.69	3.6 (D), 3.7 (H)
Ceramics						
Soda lime glass	5830	5825	5766 (Adv. NDT)	7.24	7.21	6.9 (1 Mhz, F)
B270 glass (modified soda lime)	6098	6039		3.93	3.98	7.0 (1 MHz, Schott)
Borosilicate glass	5664	5782	5610 (M), 6050 (N)	4.75	4.77	4.05 (F),4.6 (1 MHz, Q)
BK7 glass (a borosilicate glass composition)	6167	6981		3.83	3.93	4.87 para 5.45 perp (L)

(*Continued*)

Table 2. (*Continued*)

	P-wave velocity, V_p (m s^{-1})			Real relative dielectric permittivity at 10 MHz		
	Measured	Comparison	Published	Measured	Comparison	Published
Lead glass	3655	3691		12.77	12.60	7–14 (depending on K_2O content, Balaya *et al* 2004)
Fused silica	6239	6038	5900 (A)	3.90	3.97	3.7 (1 MHz C), 3.8 (D), 3.78 (F)
Silicon	8672	8537	8430 (A)			11–12 (D), 11.7–12.9 (H), 13 (10 GHz L)
Germanium	5608	5698	5410 (A)			16 (H), 16.6 (9.37 GHz L)
CaF2	6705	6765		7.01	7.04	6.81 (I),6.76 (1 MHz, K), 6.76 (1 MHz, L), 6.76 (1 MHz, Q)
Sapphire	11 315	11 641	11 913(Adv. NDT), 11100 (A)	12.35	11.90	10.55 (‖F)
Steatite	6640	5219		5.56	5.58	
Cordierite	7147	5370		4.91	4.92	
Zirconia						
Quartz (natural)	6329	6139	5740 (Adv. NDT), X-cut 5750 (A)	3.96	3.94	4.2 (D), 4.34 para 4.27 perp (30 MHz, L)
Quartz (fused)			5563 (Adv. NDT)			3.78 (E), 3.78 (F)
Alumina	10 094	9979	10 846 (Adv. NDT), 10 520 (A), 9900 (O)	10.12	10.12	9.3–11.5 (D)

Dielectric frequency response

The dielectric dispersion (figure 13) of the geological samples is significantly greater than for the engineering materials. This is attributable to vastly more complicated electrical transport processes associated with rock micro and nano-fabric creating electrical transport pathways as well additional mobile ions with small increments in moisture content (Josh 2014, Josh and Clennell 2015, Han *et al* 2016, Josh *et al* 2016). Although dry Donnybrook sandstones samples exhibit strongly dispersive behaviour, larger dispersion is observed in clay bearing rocks and shales, especially if swelling clays are present (Josh *et al* 2016). Ideally, the samples should give the same dielectric permittivity and conductance for the same sample type regardless of sample geometry and this is substantially true for the two engineering materials. Donnybrook sandstone samples are not perfectly homogenous, but the values appear to be approximately consistent. The conductivity of the Teflon is not a very useable measurement, but this is actually because the noise floor of the impedance analyser has been reached. Teflon is a well-regarded, ultra-low-loss, dielectric standard; however, in petrophysical experimentation, there are practically no geological materials that would approach the low conductivity of Teflon apart from a small number of synthetically produced geological mineral analogs, such as laboratory manufactured pure quartz, but this is outside the scope of normal usage for this instrument.

Reference material validation

Reference materials used to validate the instrument included polymers and ceramics which were suitable for both dielectric and acoustic analysis and metals which were too conductive for dielectric testing[1]. Comparison data for the reference samples was measured using commercially available instruments including a Panametrics-NDT P-wave ultrasonic test apparatus (including Olympus 5077 PR and Panametrics D7207 1 MHz transducers) and an Agilent 16451B parallel plate dielectric test fixture. The data provided in table 2 includes measurements from the present instrument, with comparison data for the same samples on the commercial instrument. Published or otherwise accepted values found in the literature or online sources have also been provided.

The measured and comparison data are in very strong agreement for both the acoustic and electrical properties and this is also true for the most part with published values. The B270 (modified soda) glass has a much higher dielectric permittivity than the published data (i.e. approximately 3.95 see 7.0), however glasses can vary significantly. For example published data indicates that the dielectric permittivity of

[1] Polymers were supplies by Dotmar plastics pty ltd; metals were provided by Robert Cameron pty ltd; natural quartz was provided by Ted Pella, germanium, silicon and CaF2 were provided by Thorlabs; remaining ceramics were provided by UqgOptics.

[2] A = www.signal-processing.com/table.php; B = www.ndt.net/links/proper.htm; C = www.glassdynamicsllc.com/bk7.html; D = www.honeywell-process.com/library/marketing/tech-specs/Dielectric%20Constant%20Table.pdf; E = www.electriciantraining.tpub.com/14193/css/Table-4-1-Dielectric-Constants-Of-Materials-138.htm; F = von hippel (1954); G = www.gplastics.com; H = www.rfcafe.com/references/electrical/dielectric-constants-strengths.htm; I = www.lightmachinery.com; K = www.sydor.com; L = www.ultiquestcom.com; M = Chocron *et al* (2009); N = Bourne *et al* (1997); O = www.ultrasonicthicknessgauges.net/sound_velocity_chart.htm; Q = www.uqgoptics.com; R = www.elcometer.com/en/velocity-chart-of-preset-materials.html; S = www.bearingworks.com/uploaded-assets/pdfs/retainers/peek-datasheet.pdf; Olymp. = www.olympus-ims.com/en/ndt-tutorials/thickness-gage/appendices-velocities/; ADV. NDT = www.advanced-ndt.co.uk/index_htm_files/Reference%20Chart%20-%20Velocity%20Chart.pdf; Schott = SCHOTT Optical Glass Datasheets.

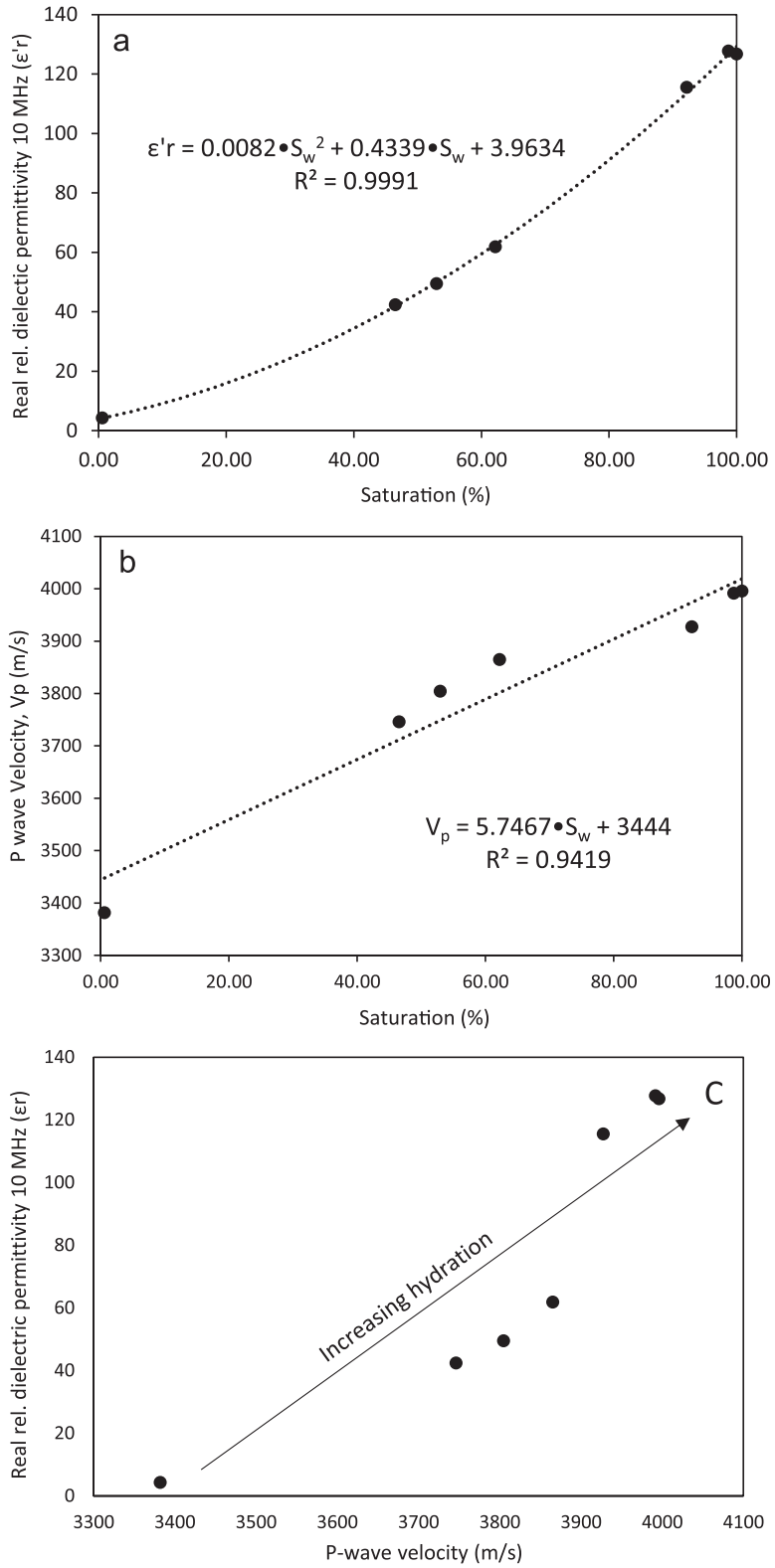

Figure 14. The (a) real relative dielectric permittivity ($R^2 = 0.999$) and (b) the P-wave velocity ($R^2 = 0.9419$) show a strong correlation with the saturation of the sample. In both cases the trends are increasing with saturation. (c) Real relative dielectric permittivity increases with an increase in P-wave velocity.

lead-glass can vary from 7 to 14 depending on its composition. In this case both measured and comparison data show that the lead-glass sample had a quite high dielectric permittivity of approximately 12.7. Even trademark branded glass such as B270 (Schott™) is not always exactly the same.

Germanium has an intriguingly high dielectric permittivity of 16 according to the published sources, however upon testing the germanium and silicon samples, they were too conductive to provide a measurement. It is likely that these samples were not pure, rather doped for semiconductor applications.

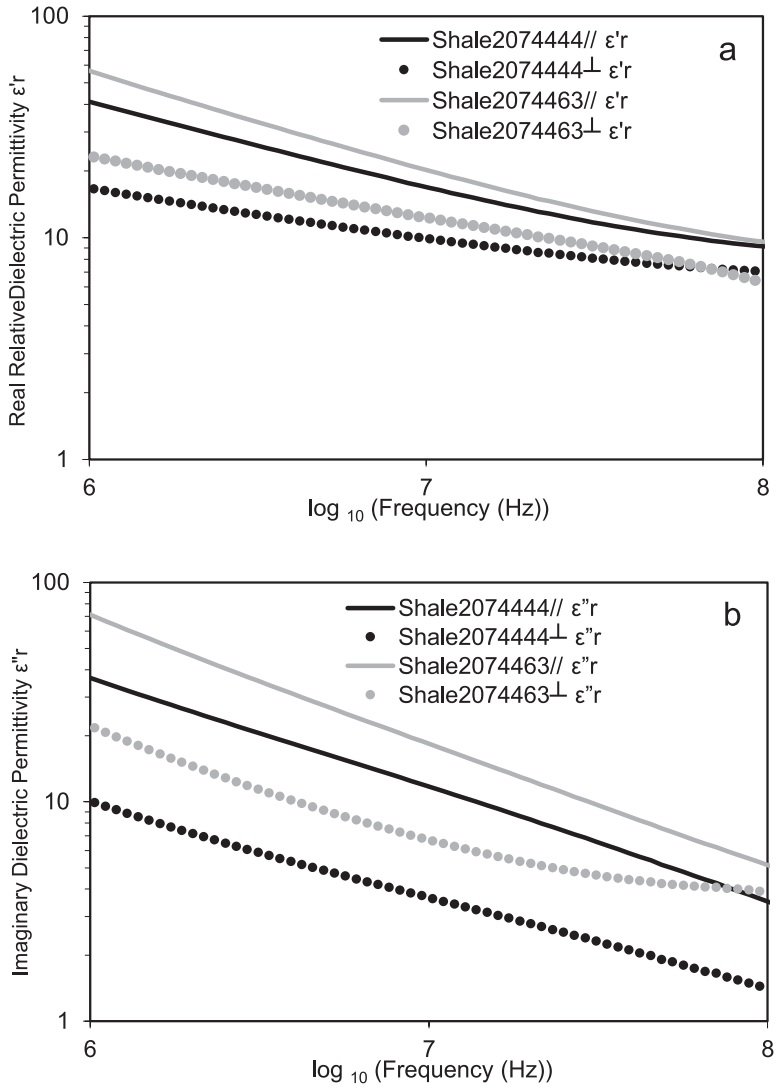

Figure 15. The (a) real and (b) imaginary dielectric permittivity of the two example shales provided are approximately 40% higher parallel (//) to bedding than orthogonal (⊥) to bedding.

Table 3. The mass and water content of a Donnybrook sandstone (9.78 mm thickness) at different levels of saturation. At full saturation, the Donnybrook sandstone reaches approximately 6.84% by mass water content.

Saturation Step	Mass (g)	Masswater (g)	Water contentby mass (%)	Saturation, S_w (%)	Real relative dielectric permittivity, ε_r at 10 MHz	P-wave velocity, V_p (m s^{-1})
Baked dry	24.06	0.00	0.00	0.00	n/a	n/a
Saturated	25.82	1.77	6.84	100.00	126.79	3995.83
Partial saturation 1	25.15	1.10	4.37	62.19	61.88	3865.08
Partial saturation 2	24.99	0.94	3.74	52.96	49.49	3804.69
Partial saturation 3	24.88	0.82	3.30	46.52	42.37	3746.15
Partial saturation 4	25.80	1.74	6.76	98.72	127.74	3991.80
Partial saturation 5	25.68	1.63	6.34	92.18	115.52	3927.42
Partial (dry) saturation	24.07	0.01	0.04	0.59	4.27	3381.94

Rock multi-hydration dielectric-acoustic response

Donnybrook sandstone is typical of conventional reservoir rock types because it has a porosity of 15.0% and fluid permeability typically of 9 mD, and may easily be saturated to different levels of hydration using the method described above. Changes in dielectric permittivity and P-wave velocity were measured on samples saturated using 35 gpl (approximate sea water) brine (table 3). The brine has a much higher dielectric permittivity than the air within the pores that it replaces and it is more dense and far more incompressible. By filling the pore-space with brine a significant change in both the P-wave velocity and bulk dielectric permittivity is anticipated from equations 1(*b*) and 2.

The dielectric permittivity increases quadratically with an increase in saturation (figure 14). The acoustic P-wave velocity increases linearly consistent the Gassmann–Hill

Table 4. The acoustic data for two example shales stabilised in 97% relative humidity which have each been plugged normal and parallel to bedding. The P-wave velocity is approximately 40% higher parallel (//) to bedding than orthogonal (⊥) to the bedding.

Sample	Sample thickness (mm)	P-wave travel time (nS)	P-wave velocity, V_p (m s^{-1})	Number of wavelengths	Real relative dielectric permittivity, ε_r at 10 MHz	Conductivity (S m^{-1})
Shale2074463 ⊥	8.18	2320.00	3525.86	10.67	12.47	3.623×10^{-3}
Shale2074463//	8.34	1680.00	4964.29	7.73	20.62	1.001×10^{-2}
Shale2074444 ⊥	8.92	2560.00	3484.38	11.78	10.02	1.978×10^{-3}
Shale2074444//	8.50	1920.00	4427.08	8.83	17.21	6.369×10^{-3}

theoretical prediction outlined in Lebedev *et al* (2009) and Müller *et al* (2010). In fact the expected relationship between P-wave velocity and saturation in Donnybrook sandstone is not previously reported however, discussion with other research scientists (Lebedev, personal communiqué) investigating this particular rock suggest that Gassmann–Hill predicts the response of Donnybrook sandstone better the Gassmann–Wood, but this is the subject of a separate discussion. A crossplot of dielectric permittivity and P-wave velocity consequently exhibits a monotonic relationship for Donnybrook sandstone (figure 14(c)), however this crossplot methodology is cautiously advised because the physical link between the two parameters is merely saturation. While both parameters may be varying due to saturation in a geological sample, salinity will affect dielectric permittivity more than P-wave velocity, and in non-porous samples such as polymers and ceramics dielectric permittivity and P-wave velocity are completely independent variables.

Anisotropy of dielectric permittivity and P-wave velocity

Shales form in a depositional environment and are naturally anisotropic. To demonstrate anisotropy of the dielectric and acoustic properties Cooper basin shales were analysed. Samples were sliced in both orientations then hydrated using a chamber at 97% relative humidity to recreate insitu conditions.

P-wave velocity in the Cooper Basin shales (stabilised at 97% relative humidity), is approximately 40% higher parallel to bedding than orthogonal (table 4). There are two reasons for this observation cited in the literature. The preferred orientation of the microcracks leads to a difference in the ability for acoustic energy to propagate in the two orientations, or 'fracture induced seismic anisotropy' (Sayers and van Munster 1991, Delle Piane *et al* 2015). This effect is significant at low confining pressures (approximately 10 MPa according to Johnston and Christensen (1995)). As the confining pressure is increased, fracture induced seismic anisotropy, is reduced as the microcracks begin to close, and above 100 MPa the observed anisotropy is mainly attributed to the alignment of the clay mineral basal planes parallel to bedding, although a small contribution from the microcracks still exists (Johnston and Christensen 1995). In the experimental data provided here (at ~6.90 MPa, table 4), both of these reasons are likely to be affecting the observed P-wave anisotropy.

Alignment of the clay basal planes with the natural bedding of the rock also affects anisotropy of the electrical transport properties. Dielectric polarisation of the unbound water existing in the pores (e.g. in sandstone such as Donnybrook presented in figure 13) exists in conjunction with multitude of additional dielectric polarisation phenomenon associated with the electrical double layer formed by the hydration of the clay mineral boundaries (Sen 1981, Revil 2013, Josh and Clennell 2015). Clays have a high specific surface area with a high density of negative charge attachment sites resulting from the exposed ends of the silicate minerals from which the clay microstructure is assembled (Bergaya *et al* 2006). With hydration, the clay boundary attracts a counter ion and leaves a mobile cation constrained to move tangentially around the silicate mineral grain and therefore aligned with the natural bedding of the rock (figure 15).

As a petrophysical tool the combination dielectric and acoustic instrument has successfully provided data for both properties consistent with previously published data. The dielectric permittivity of sandstone increases linearly with saturation at 10 MHz consistent with CRIM and the P-wave velocity in sandstone also increases with saturation consistent with the Gassmann Hill prediction. Likewise both the P-wave and dielectric permittivity observed in a shale are higher parallel to bedding than orthogonal due to the alignment of the clay mineralogy consistent with previously published research. The P-wave arrival time and the inverse of the capacitance of the dielectric cell both increase perfectly with sample thickness.

Conclusion

A new apparatus for simultaneous dielectric and acoustic analysis of rock has been developed and successfully applied to a number of engineering material standards and example rock types found in conventional petroleum system reservoirs. The new cell consists of a 3-terminal parallel plate dielectric cell using detachable electrode assemblies incorporating a P-wave transducer to create and successfully apply the world's first combination dielectric-acoustic cell for rock testing. A 4 MHz centre frequency P-wave piezo crystal was selected so that the P-wave wavelength was short enough to provide approximately 10 wavelengths across a typical parallel plate dielectric sample of 8–10 mm thickness. The new combination acoustic and dielectric cell, achieves up to 99% correlation between sample thickness versus resistance, inverse capacitance and P-wave travel time. In the geological examples investigated, the dielectric permittivity increased consistently with saturation as expected using simple mixing between rock matrix and water filled pore space. Water itself has a high dielectric permittivity compared to the rock matrix so simply mixing the two constituents together predicts an increase in bulk rock dielectric

properties with increasing water content. However, the hydration of clay bearing minerals gives rise to surfacial polarisation caused by the liberation and increased mobility of ions. In the case of highly anisotropic clay bearing rock such as shales (e.g. shale from the Cooper Basin in Australia), this manifests itself as difference in dielectric permittivity in the two orientations (i.e. orthogonal to bedding compared with parallel to bedding). P-wave velocity is also faster parallel to bedding than orthogonal, because the P-wave energy encounters less scattering interfaces and because acoustic waves propagate faster parallel to the clay basal planes which are naturally aligned in shales through compaction. Both dielectric and acoustic anisotropy can easily be determined using a pair of matched orthogonal samples. Saturation also affects the P-wave velocity differently in each sample. In the case of Donnybrook sandstone, increasing saturation leads to a nearly linear increase in P-wave velocity consistent with the Gassmann Hill theory.

The real advantage of this instrument is that variations in geological material would normally cause a discrepancy between the dielectric analysis and the acoustic analysis which is achieved with separate measurements on possibly two separate samples in different states of hydration, or heterogeneity in mineralogy, porosity or microstructure. With this instrument, real and imaginary dielectric permittivity, conductivity and P-wave velocity are all determined in one rapid measurement, which is a significant advance in the state of the art for petrophysical joint dielectric and acoustic analysis.

Acknowledgments

I would like to acknowledge Stuart Dahl for instrument manufacture, Tony Siggins, Rod Banks and Greg Lupton for previous componentry of the load arrangement, Tongcheng Han and Lionel Esteban for sample preparation and experimental input. Maxim Lebedev, Joel Sarout, Alexy Yurikov and Claudio Delle Piane for knowledge relating to acoustic measurement. I would also like to thank David Dewhurst, Tobias Müller, Claudio Delle Piane, Maxim Lebedev and Emma Josh, for their invaluable help with editing. Marina Pervukhina and Ben Clennell for their helpful assistance. Wayne Murray for knowledge relating to three terminal capacitor design. Neil Sturrock, Derek Winchester and Dave Walton for technical assistance.

ORCID iDs

Matthew Josh https://orcid.org/0000-0002-4082-0447

References

Archie G E 1941 The electrical resistivity log as an aid in determining some reservoir characteristics *Trans. AIME* **146** 54–62

Asami K 2002 Characterization of heterogeneous systems by dielectric spectroscopy *Prog. Polym. Sci.* **27** 1617–59

ASTM 2000 S Designation D2845-00: Standard test method for laboratory determination if pulse velocities and ultrasonic elastic constants of rock (West Conshohocken, PA: ASTM International)

Balaya P, Shrikhande V K, Kothiyal G P and Goyal P S 2004 Dielectric and conductivity studies on lead silicate glasses having mixed alkali and alkaline earth metal oxides *Curr. Sci.* **86** 553–6

Bergaya F, Theng B K G and Lagaly G 2006 *Handbook of Clay Science* (Amsterdam: Elsevier) p 1224

Birchak J R, Gardner C G, Hipp J E and Victor J M 1974 High dielectric constant microwave probes for sensing soil moisture *Proc. IEEE* **62** 93–8

Bourne N, Forde L, Millett J and Field J 1997 Impact and penetration of a borosilicate glass *J. Phys. Colloq.* **07** C3-157–62

Bruggeman D A G 1935 Berechnung verschiedener physikalischer Konstanten von heterogenen Substanzen. I. Dielektrizitätskonstanten und Leitfähigkeiten der Mischkörper aus isotropen Substanzen *Ann. Phys.* **416** 636–64

Chocron S, Anderson C E, Dannemann K A and Nicholls A E 2009 Characterization of borosilicate glass through confined compression testing with numerical validation *Report* 18.12544/010 US Army AMSRD-TAR-R, Warren, MI

Delle Piane C, Almqvist B S G, MacRae C M, Torpy A, Mory A J and Dewhurst D N 2015 Texture and diagenesis of Ordovician shale from the Canning Basin, Western Australia: implications for elastic anisotropy and geomechanical properties *Mar. Pet. Geol.* **59** 56–71

Ellis D V and Singer J M 2007 *Well Logging for Earth Scientists* (Berlin: Springer)

Fuller B D and Ward S H 1970 Linear system description of electrical parameters of rocks *IEEE Trans. Geosci. Electron.* **GE-8** 7–18

Gassmann F 1951 *Über die Elastizität Poröser Medien* vol 96 (Zürich: Viertel. Naturforsch. Ges.) pp 1–23

Guéguen Y and Palciauskas V 1994 *Introduction to the Physics of Rocks* (Princeton, NJ: Princeton University Press) 392p

Han T, Clennell M B, Pervukhina M and Josh M 2016 Saturation effects on the joint elastic-dielectric properties of carbonates *J. Appl. Geophys.* **129** 36–40

Hanai T 1960 Theory of dielectric dispersion due to the interfacial polarization and its application to emulsions *Colloid Polym. Sci.* **171** 23–31

Ishai P B, Talary M S, Caduff A, Levy E and Feldman Y 2013 Electrode polarization in dielectric measurements: a review *Meas. Sci. Technol.* **24** 102001

Johnston J E and Christensen N I 1995 Seismic anisotropy of shales *J. Geophys. Res.* **100** 5991–6003

Josh M 2014 Dielectric permittivity: a petrophysical parameter for shales *Petrophysics* **55** 319–32

Josh M 2017 Dielectric and acoustic properties with a single laboratory instrument *Society of Core Analysts: SCA Conf. (Vienna, Austria, August)* paper number 99

Josh M and Clennell B 2015 Broadband electrical properties of clays and shales: comparative investigation of remoulded and preserved samples *Geophysics* **80** D129–43

Josh M, Clennell B and Siggins T 2009 Practical broadband dielectric measurement of geological samples *50th SPWLA Annual Logging Symp. (Woodlands, TX, 21–24 June)*

Josh M, Clennell B, Cauchefert M P and Han T 2016 Dielectric permittivity and anisotropy of intact multi-saturated organic shales *57th SPWLA Annual Logging Symp. (Reykjavic, Iceland, 25–29 June)*

Josh M, Clennell B, Siggins T and Banks R 2007 Wideband electrical/dielectric measurements from millihertz to gigahertz

frequencies *77th Annual Meeting of the SEG (San Antonio, USA)* pp 1701–5
Keysight Technologies 2008 16451b dielectric test fixture, operation and service manual (Japan: Agilent Technologies)
Keysight Technologies 2017 Basics of measuring the dielectric properties of materials, application note 5989-2589EN (USA: Keysight Technologies)
Lebedev M, Toms-Stewart J, Clennell B, Pervukhina M, Shulakova V, Paterson L, Müller T, Gurevich B and Wenzlau F 2009 Direct laboratory observation of patchy saturation and its effects on ultrasonic velocities *Leading Edge* **28** 24–8
Malleo D, Nevill J T, van Ooyen A, Schnakenberg U, Lee L P and Morgan H 2010 Note: Characterization of electrode materials for dielectric spectroscopy *Rev. Sci. Instrum.* **81** 016104
Mazzagatti R P, Dowling D J, Sims J C, Bussian A E and Simpson R S 1983 Laboratory measurement of dielectric constant near 20 MHz *SPE 12097 56th Annual Technical Conf. and Exhibition (San Francisco, 5th–8th October)*
Meador R A and Cox P T 1975b Dielectric constant logging, a salinity independent estimation of formation water volume *Paper SPE 5504 Presented at the 50th Annual Technical Conf. (Dallas Texas, 28 October)*
Meador R A, Arnold R H and Paap H J 1975a Dual radio frequency measurement of dielectric constant and resistivity of borehole media *US Patent* No. 3891916
Müller T M, Gurevich B and Lebedev M 2010 Seismic wave attenuation and dispersion resulting from wave-induced flow in porous rocks—a review *Geophysics* **75** 75A147–64
Myers M T 1991 A saturation interpretation model for the dielectric constant of shaly sands *Int. Symp. Society of Core Analysts: SCA Conf. (San Antonio, USA)* paper 9118
Rae P J and Brown E N 2016 Some observations on measuring sound speeds in polymers using time-of-flight *Exp. Tech.* **40** 1085–97
Revil A 2013 Effective conductivity and permittivity of unsaturated porous materials in the frequency range 1 mHz–1 GHz *Water Resour. Res.* **49** 306–27
Sayers C M and van Munster J G 1991 Micro-induced seismic anisotropy of sedimentary rocks *J. Geophys. Res.* **96** 16529–33
Seleznev N V, Kleinberg R L, Herron M M, Machlus M, Pomerantz A E, Reeder S L, Burnham A K, Day R L and Allix P C 2011 Applications of dielectric dispersion logging to oil-shale reservoirs *SPWLA 52nd Annual Logging Symp. (Colorado Springs, CO, 14–18 May)* paper G
Sen P N, Scala C and Cohen M H 1981 A self-similar model for sedimentary rocks with application to the dielectric constant of fused glass beads *Geophysics* **46** 781–95
Siggins A F, Gunning J and Josh M 2011 A hybrid waveguide cell for dielectric properties of reservoir rocks *Meas. Sci. Technol.* **22** 025702
Sihvola A H 1999 *Electromagnetic Mixing Formulas and Applications* (London: The Institution of Engineering and Technology)
Von Hippel A R 1954 *Dielectric Materials and their Applications* (Cambridge, MA: The Technology Press of MIT)